


**Angle-resolved pair photoemission theory for correlated electrons**

Thomas P. Devereaux <sup>1,2,3,\*</sup> Martin Claassen,<sup>4</sup> Xu-Xin Huang,<sup>1</sup> Michael Zaletel,<sup>5,6</sup> Joel E. Moore,<sup>5,6</sup> Dirk Morr,<sup>7</sup> Fahad Mahmood,<sup>8</sup> Peter Abbamonte,<sup>8</sup> and Zhi-Xun Shen<sup>1,2,9</sup>

<sup>1</sup>*Stanford Institute for Materials and Energy Sciences, SLAC National Accelerator Laboratory, 2575 Sand Hill Road, Menlo Park, California 94025, USA*

<sup>2</sup>*Geballe Laboratory for Advanced Materials, Stanford University, Stanford, California 94305, USA*

<sup>3</sup>*Department of Materials Science and Engineering, Stanford University, Stanford, California 94305, USA*

<sup>4</sup>*Department of Physics and Astronomy, University of Pennsylvania, Philadelphia, Pennsylvania 19104, USA*

<sup>5</sup>*Department of Physics, University of California, Berkeley, California 94720, USA*

<sup>6</sup>*Materials Sciences Division, Lawrence Berkeley National Laboratory, Berkeley, California 94720, USA*

<sup>7</sup>*University of Illinois at Chicago, Chicago, Illinois 60607, USA*

<sup>8</sup>*University of Illinois at Urbana Champaign, Champaign, Illinois 61801, USA*

<sup>9</sup>*Departments of Physics and Applied Physics, Stanford University, Stanford, California 94305, USA*



(Received 12 August 2023; revised 2 October 2023; accepted 5 October 2023; published 18 October 2023)

In this paper, we consider the possibility and conditions for pair photoemission, whereby two incident photons emit pairs of electrons from a candidate material, as a method to measure and visualize electronic correlations. As opposed to double photoemission—where a single photon precipitates the ejection of a pair of electrons via a subsequent electron energy loss scattering process—we show that pair photoemission need not be limited to interference between initial photoelectrons and valence electrons and moreover can occur without the energy penalty of two work functions. This enables detection of pairs of electrons at high-energy resolution that may be correlated in the same quantum many-body states.

DOI: [10.1103/PhysRevB.108.165134](https://doi.org/10.1103/PhysRevB.108.165134)

**I. INTRODUCTION**

Over the past decades, angle-resolved photoemission spectroscopy (ARPES) has emerged as a paradigmatic experimental probe of electronic structure and correlations, band topology or surface states, unconventional superconductivity or the enigmatic pseudogap phase, granting insight into characterizing electronic behavior in quantum materials. By measuring the kinetic energy and angular dependence of photoemitted electrons, ARPES supplies information on the energy and momentum dependence of valence electrons in a material and is widely understood to reflect a good approximation of the behavior of the single-particle spectral function [1].

Higher-order photoemission processes have been utilized to further obtain information beyond the single-particle density of states. In double photoemission, for example, a highly energetic photon causes the emission of an electron which may cause a second electron to be photoemitted via the Coulomb interaction if it can impart enough energy for the second electron to escape to a detector [2]. For example, a photoemitted core electron may be accompanied by Auger electron emission, whereby the energy emitted by Auger decay of the core hole is utilized to cause another electron to be emitted [3]. Such shake-off or secondaries spectra contain both photoemitted core and Auger electrons. The

fact that the energies of the two electrons can be themselves continuous yet sum to conserve energy can show that the electrons are correlated, and a comparison with single-particle photoemission can be utilized to determine the so-called exchange-correlation hole energy and momentum-space structure [4,5].

In analogy to photon- or electron-based coincidence spectroscopies, recently, an interesting proposal suggested extending ARPES to use energy and angle-resolved coincidence detection to account for two-photon, two-electron photoemission events and extract two-particle Bethe-Salpeter wave functions [6] of valence electrons of the material. Here, in contrast with double photoemission due to Coulomb drag, the coincidence signal derives from two-photon absorption at lower photon energies. Measurement of the angle dependence of two-photon coincidence events at the detector hence importantly permits resolving the momenta and energies of the ejected electron pairs, without the need to disentangle highly complex Coulomb drag processes that complicate the study of important low-energy effects.

While the possibility to extract electronic correlations from coincidence counts in ARPES immediately suggests a variety of applications such as elucidating unconventional pairing mechanisms in high-temperature superconductors or heavy-fermion compounds, a key question concerns understanding exactly the nature of what this probe actually measures in a correlated electron system and how to interpret its result in terms of more intuitive quantities such as pair correlation functions or the superconducting gap. Indeed, it is

\*tpd@stanford.edu

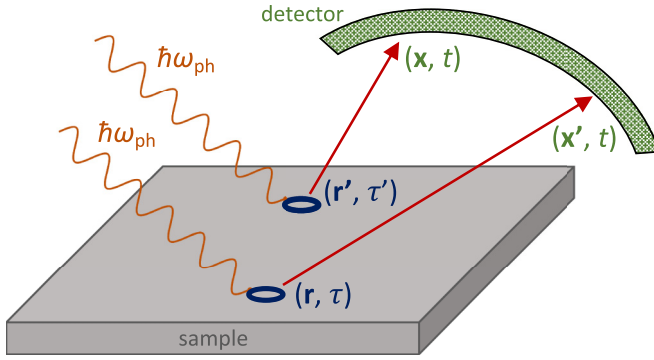


FIG. 1. Setup: Two electrons at  $(\bar{\mathbf{r}}, \tau)$ ,  $(\bar{\mathbf{r}}', \tau')$  are photoemitted upon absorbing two photons with frequency  $\omega_{\text{ph}}$ . Coincidence detection takes place at time  $t$  and positions  $\mathbf{x}$ ,  $\mathbf{x}'$ .

straightforward to see that the coincidence signal does not map onto more readily interpretable superconducting pair correlation functions since pairs of detected electrons that comprise a coincidence signal are not necessarily ejected from the sample at the same time. On the other hand, a more microscopic description of the pair ARPES cross-section is necessary to permit a formal accounting for final-state effects and the detector geometry and differentiate from double photoemission.

In this paper, we address these questions by developing a generic theoretical description of angle-resolved pair photoemission and studying its behavior in light of superconducting instabilities in the attractive and repulsive Hubbard model on small clusters. We show that pair photoemission need not be limited to interference between initial photoelectrons and valence electrons and moreover can occur without the energy penalty of two work functions. This enables detection of pairs of electrons at high-energy resolution that may be correlated in the same quantum many-body states.

Figure 1 depicts a schematic of the pair photoemission process for a two-dimensional sample or surface state. Two photons with energy  $\hbar\omega_{\text{ph}}$  eject two electrons from the sample, which are subsequently observed at the detector at the same time  $t$  with both angle and energy resolution. For simplicity but without loss of generality, we ignore bulk effects and henceforth denote three-dimensional positions and momenta using bold notation  $\mathbf{r}$ , whereas their two-dimensional components in the sample plane are denoted by  $\bar{\mathbf{r}}$ . Suppose that sample and emitted electrons are described by fields  $\hat{\Phi}(\bar{\mathbf{r}})$  and  $\hat{\Psi}(\mathbf{r})$ , respectively (we suppress implicit spin indices, for conciseness), and are governed by a generic Hamiltonian  $\hat{H}$ :

$$\hat{H}_0 = \hat{H}_{\text{valence}}(\hat{\Phi}) + \hat{H}_{\text{emitted}}(\hat{\Psi}) + \hat{H}_{\text{v-e}}(\hat{\Phi}, \hat{\Psi}), \quad (1)$$

such that emitted electrons  $\hat{\Psi}$  behave as freely propagating waves at long distances from the sample while appropriately encapsulating final-state effects [time-reversed low-energy electron diffraction (LEED)] as well as possible back actions  $\hat{H}_{\text{v-e}}(\hat{\Phi}, \hat{\Psi})$  which would be important for Coulomb-drag-mediated double photoemission.

The photoemission process  $\hat{H}_{\text{el-ph}}$  in the rotating-wave approximation now takes a sample electron  $\hat{\Phi}(\bar{\mathbf{r}})$  to a prop-

agating final state  $\hat{\Psi}(\mathbf{r})$ :

$$\begin{aligned} \hat{H}_{\text{el-ph}}(t) = & s(t) \int d^3\mathbf{r} g(\mathbf{r}) \hat{\Psi}^\dagger(\mathbf{r}) \hat{\Phi}(\bar{\mathbf{r}}) \\ & \times \exp(-i\omega_{\text{ph}}t) + \text{H.c.}, \end{aligned} \quad (2)$$

where  $g(\mathbf{r}) = e\mathbf{r} \cdot \mathbf{E}_0$  describes photoemission in dipole gauge with  $\phi = \mathbf{r} \cdot \mathbf{E}(t)$ ,  $\mathbf{A} = 0$  for an electric field  $\mathbf{E}(t) = \mathbf{E}_0 \cos(\omega_{\text{ph}}t)$ , and  $s(t)$  describes a Gaussian probe pulse envelope with

$$s(t) = \exp\left[-\frac{(t-t_0)^2}{2\sigma_{\text{pr}}^2}\right]. \quad (3)$$

Subsequently, the photoelectron detector measures the mean momentum  $\mathbf{k}$  of propagating electron wave packets, described by a photocurrent:

$$\langle \hat{J}_{\mathbf{k}} \rangle = \frac{\mathbf{k}}{e} \iint d\mathbf{x} d\mathbf{x}' \phi_{\mathbf{k}}^*(\mathbf{x}) \phi_{\mathbf{k}}(\mathbf{x}') \langle \hat{\Psi}^\dagger(\mathbf{x}) \hat{\Psi}(\mathbf{x}') \rangle, \quad (4)$$

where  $\phi_{\mathbf{k}}(\mathbf{r})$  denotes a wave packet centered at the detector location [7].

## II. FORMALISM

### A. Single-electron ARPES

The conventional single-electron ARPES signal now follows straightforwardly [7] from a perturbative expansion in  $\hat{H}_{\text{el-ph}}$  of the measured photocurrent:

$$\begin{aligned} I_{\mathbf{k}} = & \int_{-\infty}^t d\tau d\tau' s(\tau) s(\tau') \exp[i\omega_{\text{ph}}(\tau - \tau')] \\ & \times \int d\mathbf{x} d\mathbf{x}' \phi_{\mathbf{k}}^*(\mathbf{x}) \phi_{\mathbf{k}}(\mathbf{x}') \int d\bar{\mathbf{r}} d\bar{\mathbf{r}}' g^*(\bar{\mathbf{r}}) g(\bar{\mathbf{r}}') \\ & \times \langle \hat{\Phi}^\dagger(\bar{\mathbf{r}}, \tau) \hat{\Psi}(\mathbf{r}, \tau) \hat{\Psi}^\dagger(\mathbf{x}, t) \hat{\Psi}(\mathbf{x}', t) \hat{\Psi}^\dagger(\mathbf{r}', \tau') \hat{\Phi}(\bar{\mathbf{r}}', \tau') \rangle, \end{aligned} \quad (5)$$

where  $\langle \cdot \rangle = \text{tr}\{\cdot \exp(-\beta\hat{H}_0)\}/Z$  denotes thermal expectation values with respect to  $\hat{H}_0$ . If back-action  $\hat{H}_{\text{v-e}}$  between emitted and valence electrons can be neglected, this expression simplifies drastically, as  $\langle \hat{\Phi}^\dagger(\bar{\mathbf{r}}, \tau) \hat{\Psi}(\mathbf{r}, \tau) \hat{\Psi}^\dagger(\mathbf{x}, t) \hat{\Psi}(\mathbf{x}', t) \hat{\Psi}^\dagger(\mathbf{r}', \tau') \hat{\Phi}(\bar{\mathbf{r}}', \tau') \rangle = \langle \hat{\Phi}^\dagger(\bar{\mathbf{r}}, \tau) \hat{\Phi}(\bar{\mathbf{r}}', \tau') \rangle \langle \hat{\Psi}(\mathbf{r}, \tau) \hat{\Psi}^\dagger(\mathbf{x}, t) \rangle \langle \hat{\Psi}(\mathbf{x}', t) \hat{\Psi}^\dagger(\mathbf{r}', \tau') \rangle$ . Furthermore, assuming a single electronic valence band  $\hat{\Phi}(\bar{\mathbf{r}}) = \sum_{\bar{\mathbf{k}}} u_{\bar{\mathbf{k}}}(\bar{\mathbf{r}}) e^{i\bar{\mathbf{k}}\bar{\mathbf{r}}} \hat{c}_{\bar{\mathbf{k}}}$  with Bloch function  $u_{\bar{\mathbf{k}}}(\bar{\mathbf{r}})$ , and neglecting the detector wave packet shape functions  $\phi_{\mathbf{k}}(\mathbf{x}) \rightarrow e^{i\mathbf{k}\mathbf{x}}$  [thereby discarding time-of-flight (TOF) information], one arrives at ( $\mathbf{k} \rightarrow \mathbf{k}$ ):

$$\begin{aligned} I_{\mathbf{k}} = & -i \int_{-\infty}^t d\tau d\tau' \exp[i\omega_{\text{ph}}(\tau - \tau')] s(\tau) s(\tau') |M_{\mathbf{k}}|^2 \\ & \times G_{\bar{\mathbf{k}}}^<(\tau, \tau') \mathcal{G}_{\bar{\mathbf{k}}}^*(\tau, t) \mathcal{G}_{\bar{\mathbf{k}}}(t, \tau'), \end{aligned} \quad (6)$$

where  $M_{\mathbf{k}} = \int d\mathbf{r} \chi_{\bar{\mathbf{k}}}^*(\mathbf{r}) g(\mathbf{r}) u_{\bar{\mathbf{k}}}(\mathbf{r}) e^{i\mathbf{k}\mathbf{r}}$  is a matrix element evaluated from  $g(\mathbf{r})$ , the Bloch function of the single valence band, and the time-reversed LEED wave function  $\chi_{\bar{\mathbf{k}}}(\mathbf{r})$ . Here,

$G_{\mathbf{k}}^{\leq}(\tau, \tau')$  is the lesser sample Green's function:

$$G_{\mathbf{k}}^{\leq}(\tau, \tau') = i\langle \hat{c}_{\mathbf{k}}^{\dagger}(\tau)\hat{c}_{\mathbf{k}}(\tau') \rangle, \quad (7)$$

and

$$\mathcal{G}_{\mathbf{k}}(t, t') = -i\langle \hat{T}\hat{c}_{\mathbf{k}}(t)\hat{c}_{\mathbf{k}}^{\dagger}(t') \rangle \quad (8)$$

is the propagating electron Green's function for a time-reversed LEED state. Finally, a drastically simplified expression can be provided if  $\mathcal{G}_{\mathbf{k}}$  is approximated by a free-electron Green's function with dispersion  $\epsilon_{\mathbf{k}} = \mathbf{k}^2/2m_0$ . Then defining the kinetic energy  $\omega$  observed at the detector as

$$\omega \equiv \omega_{\text{ph}} - \frac{\mathbf{k}^2}{2m_0} - W, \quad (9)$$

where  $W$  is the work function of the sample, and taking  $t \rightarrow \infty$ , one finally arrives at

$$I_{\mathbf{k}} = i \int_{-\infty}^{\infty} d\tau d\tau' \exp[i\omega(\tau - \tau')] s(\tau)s(\tau') |M_{\mathbf{k}}|^2 G_{\mathbf{k}}^{\leq}(\tau, \tau'). \quad (10)$$

This is the usual expression for single-particle ARPES in terms of convolutions of shape functions, matrix elements, and the lesser Green's function [7].

### B. Angle-resolved pair photoemission

Similarly, a coincidence measurement signal can be defined by generalizing Eq. (4) and Ref. [7] to the detection of a

pair of electrons:

$$\begin{aligned} \langle \hat{J}_{\mathbf{k}_1\mathbf{k}_2} \rangle &= \frac{\mathbf{k}_1\mathbf{k}_2}{e^2} \int d\mathbf{x}_1 d\mathbf{x}'_1 d\mathbf{x}_2 d\mathbf{x}'_2 \phi_{\mathbf{k}_1}^*(\mathbf{x}_1) \phi_{\mathbf{k}_2}^*(\mathbf{x}'_1) \phi_{\mathbf{k}_2}(\mathbf{x}'_2) \\ &\times \sum_{\nu\nu'} \phi_{\mathbf{k}_1}(\mathbf{x}_2) \langle \hat{\Psi}_{\nu}^{\dagger}(\mathbf{x}_1, t) \hat{\Psi}_{\nu'}^{\dagger}(\mathbf{x}'_1, t) \hat{\Psi}_{\nu'}(\mathbf{x}'_2, t) \hat{\Psi}_{\nu}(\mathbf{x}_2, t) \rangle. \end{aligned} \quad (11)$$

Here, we restore spin indices  $\nu, \nu'$  and model a spin-agnostic detector. In complete analogy to single-electron ARPES, the photodetection rate can now be evaluated from a perturbative expansion in  $\hat{H}_{\text{el-ph}}$ . To first order, the response involves a single photoemission vertex and vanishes. We note that this contribution is essential for Coulomb-mediated double photoemission (a single absorbed photon effectively ejects a pair of electrons) for high photon energies. Here, a perturbative expansion in  $\hat{H}_{\text{v-e}}(\hat{\Phi}, \hat{\Psi})$  additionally accounts for the Coulomb interaction mediated back action of the photoemitted electron, imparting enough energy on a second sample electron to eject it, rendering the coincidence signal nonzero. As discussed above, we are primarily interested in two-photon, two-electron pair ARPES processes at lower photon energy; in this regime, the double emission contribution is negligible for energetic reasons, provided that the photon energy is less than twice the ionization energy.

To second order in  $\hat{H}_{\text{el-ph}}$ , the two-photon, two-electron coincidence photodetection signal formally reads

$$\begin{aligned} D_{\mathbf{k}_1\mathbf{k}_2} &= \sum_{\substack{\sigma_1\sigma'_1\nu \\ \sigma_2\sigma'_2\nu'}} \int_{-\infty}^t d\tau_1 d\tau_2 \int_{-\infty}^{\tau_1} d\tau'_1 \int_{-\infty}^{\tau_2} d\tau'_2 \exp[i\omega_{\text{ph}}(\tau_1 + \tau'_1 - \tau_2 - \tau'_2)] s(\tau_1)s(\tau'_1)s(\tau_2)s(\tau'_2) \\ &\times \int d\mathbf{r}_1 d\mathbf{r}'_1 d\mathbf{r}_2 d\mathbf{r}'_2 g^*(\mathbf{r}_1)g^*(\mathbf{r}'_1)g(\mathbf{r}_2)g(\mathbf{r}_2) \int d\mathbf{x}_1 d\mathbf{x}'_1 d\mathbf{x}_2 d\mathbf{x}'_2 \phi_{\mathbf{k}_1}^*(\mathbf{x}_1) \phi_{\mathbf{k}_2}^*(\mathbf{x}'_1) \phi_{\mathbf{k}_2}(\mathbf{x}'_2) \phi_{\mathbf{k}_1}(\mathbf{x}_2) \\ &\times \langle \hat{\Phi}_{\sigma_1}^{\dagger}(\mathbf{r}_1, \tau_1) \hat{\Psi}_{\sigma_1}(\mathbf{r}_1, \tau_1) \hat{\Phi}_{\sigma'_1}^{\dagger}(\mathbf{r}'_1, \tau'_1) \hat{\Psi}_{\sigma'_1}(\mathbf{r}'_1, \tau'_1) \hat{\Psi}_{\nu}^{\dagger}(\mathbf{x}_1, t) \hat{\Psi}_{\nu'}^{\dagger}(\mathbf{x}'_1, t) \hat{\Psi}_{\nu'}(\mathbf{x}'_2, t) \hat{\Psi}_{\nu}(\mathbf{x}_2, t) \\ &\times \hat{\Psi}_{\sigma'_2}^{\dagger}(\mathbf{r}'_2, \tau'_2) \hat{\Phi}_{\sigma'_2}(\mathbf{r}'_2, \tau'_2) \hat{\Psi}_{\sigma_2}^{\dagger}(\mathbf{r}_2, \tau_2) \hat{\Phi}_{\sigma_2}(\mathbf{r}_2, \tau_2) \rangle. \end{aligned} \quad (12)$$

Assuming negligible back action or Coulomb interactions between photoemitted electrons and low-energy sample electrons, this daunting multipoint correlation function can be decomposed in analogy to conventional ARPES. The coincidence detection rate can be written as

$$\begin{aligned} D_{\mathbf{k}_1\mathbf{k}_2} &= \int_{-\infty}^t d\tau_1 d\tau_2 \int_{-\infty}^{\tau_1} d\tau'_1 \int_{-\infty}^{\tau_2} d\tau'_2 s(\tau_1)s(\tau'_1)s(\tau_2)s(\tau'_2) \int d\mathbf{k} d\mathbf{k}' d\mathbf{q} \sum_{\substack{\sigma_1\sigma'_1\nu \\ \sigma_2\sigma'_2\nu'}} G_{\mathbf{k}\mathbf{k}'\mathbf{q}}^{\sigma_1\sigma'_2}(\tau_1, \tau'_1, \tau'_2, \tau_2) \\ &\times \exp[i\omega_{\text{ph}}(\tau_1 + \tau'_1 - \tau_2 - \tau'_2)] [F_{\mathbf{k}\mathbf{q}}^{\sigma_1\sigma'_1\nu\nu'}(\tau_1, \tau'_1)]^* F_{\mathbf{k}'\mathbf{q}}^{\sigma_2\sigma'_2\nu\nu'}(\tau_2, \tau'_2), \end{aligned} \quad (13)$$

where

$$G_{\mathbf{k}\mathbf{k}'\mathbf{q}}^{\sigma\nu}(\tau_1, \tau'_1, \tau'_2, \tau_2) = \langle \hat{c}_{\mathbf{k}\sigma}^{\dagger}(\tau_1) \hat{c}_{\mathbf{q}-\mathbf{k}\sigma'}^{\dagger}(\tau'_1) \hat{c}_{\mathbf{q}-\mathbf{k}'\nu'}(\tau'_2) \hat{c}_{\mathbf{k}'\nu}(\tau_2) \rangle \quad (14)$$

is the two-particle Green's function for the sample, and

$$F_{\mathbf{k}\mathbf{q}}^{\sigma\sigma'\nu\nu'}(\tau, \tau') = \int d\mathbf{p} d\mathbf{p}' \phi_{\mathbf{k}_1}(\mathbf{p}) \phi_{\mathbf{k}_2}(\mathbf{q} - \mathbf{p}) M_{\mathbf{q}-\mathbf{k}} M_{\mathbf{k}} \langle 0 | \hat{\Psi}_{\mathbf{p}\nu'}(t) \hat{\Psi}_{\mathbf{q}-\mathbf{p}\nu}(t) \hat{\Psi}_{\mathbf{q}-\mathbf{k}\sigma'}^{\dagger}(\tau') \hat{\Psi}_{\mathbf{k}\sigma}^{\dagger}(\tau) | 0 \rangle \quad (15)$$

is a four-point function for the photoemitted electrons which includes the Fourier-transformed detector shape functions  $\phi_{\mathbf{k}}(\cdot)$  and is evaluated with respect to the vacuum state. Furthermore,  $M_{\mathbf{k}}$  denote photoexcitation matrix elements defined in terms of the dipole matrix element and valence electron Bloch functions introduced above. Here,  $F_{\mathbf{k}\mathbf{q}}(\tau, \tau')$  encodes both propagation and TOF information as well as interactions between the two photoemitted electrons. A drastic simplification follows from treating emitted electrons as free fermions. In this case,  $F_{\mathbf{k}\mathbf{q}}(\tau, \tau')$  factorizes to

$$F_{\mathbf{k}\mathbf{q}}(\tau, \tau') = M_{\mathbf{q}-\mathbf{k}}M_{\mathbf{k}} \exp\{-i[\epsilon_{\mathbf{k}}(t - \tau) + \epsilon_{\mathbf{q}-\mathbf{k}}(t - \tau')]\} \\ \times [\phi_{\mathbf{k}_1}(\mathbf{k})\phi_{\mathbf{k}_2}(\mathbf{q} - \mathbf{k})\delta_{\sigma, \nu'}\delta_{\sigma', \nu} \\ - \phi_{\mathbf{k}_2}(\mathbf{k})\phi_{\mathbf{k}_1}(\mathbf{q} - \mathbf{k})\delta_{\sigma, \nu}\delta_{\sigma', \nu}], \quad (16)$$

where  $\epsilon_{\mathbf{k}} = \mathbf{k}^2/2m_0$  is the dispersion of the photoemitted electrons. This expression generalizes the formalism of Ref. [6] to, in principle, include TOF information and interactions between the photoemitted electrons. In analogy to the theory for conventional ARPES [7], we can now make the assumption that the detector wave packet momentum width can be neglected  $\phi_{\mathbf{k}}(\mathbf{k}) \rightarrow \delta(\mathbf{k} - \mathbf{k})$ , discarding again TOF information and dependence on the detector position. Denote the energies observed at the two detectors minus the photon energy as

$$\omega_{1,2} \equiv \omega_{\text{ph}} - \frac{\mathbf{k}_{1,2}^2}{2m_0} - W, \quad (17)$$

with  $W$  the work function of the sample, and taking  $t \rightarrow \infty$ , the coincidence detection rate can be written as

$$D_{\mathbf{k}_1\mathbf{k}_2}^{(0)} = \int_{-\infty}^{\infty} d\tau_1 d\tau'_1 d\tau_2 d\tau'_2 \\ \times s(\tau_1)s(\tau'_1)s(\tau_2)s(\tau'_2) \sum_{\sigma\sigma'} G_{\mathbf{k}_1, \mathbf{k}_2, \sigma, \sigma'}^{(2)} \\ \times \exp[i\{\omega_1(\tau_1 - \tau_2) + \omega_2(\tau'_1 - \tau'_2)\}], \quad (18)$$

where

$$G_{\mathbf{k}_1, \mathbf{k}_2, \sigma, \sigma'}^{(2)} = \langle \hat{T} \hat{c}_{\mathbf{k}_1\sigma}^\dagger(\tau_1) \hat{c}_{\mathbf{k}_2\sigma'}^\dagger(\tau'_1) \hat{T} \hat{c}_{\mathbf{k}_2\sigma'}(\tau_2) \hat{c}_{\mathbf{k}_1\sigma}(\tau_2) \rangle, \quad (19)$$

and  $\hat{T}$  denotes time ordering, and we additionally omitted the photoexcitation matrix elements  $M_{\mathbf{k}}$  for conciseness. This simplified expression recovers the results of Ref. [6].

### C. Fermi's golden rule

This expression can be recast into the more familiar Fermi's golden rule by inserting complete sets of the states for the  $N, N - 1$ , and  $N - 2$  particle sectors. Also, if we neglect the time dependence of the shape functions so that we only concentrate on frequency resolution, the time integrals can be performed, and the following expression is obtained:

$$D_{\mathbf{k}_1, \mathbf{k}_2}^{(0)}(\omega_1, \omega_2) = \sum_n |M_{0,n}(\mathbf{k}_1, \mathbf{k}_2, \omega_1, \omega_2)|^2 \\ \times \delta(E_n - E_0 + \omega_1 + \omega_2), \quad (20)$$

with  $E_0$  denoting the  $N$  particle ground-state energy and  $E_n$  the eigenenergies of the  $N - 2$  particle sector, viz., the expression

is simply a matrix element squared times a term that enforces energy conservation. The matrix element reads

$$M_{0,n}(\mathbf{k}_1, \mathbf{k}_2, \omega_1, \omega_2) = \sum_{m, \sigma_1, \sigma_2} \left\{ \frac{\langle n | \hat{c}_{\mathbf{k}_2\sigma_2} | m \rangle \langle m | \hat{c}_{\mathbf{k}_1\sigma_1} | 0 \rangle}{E_m - E_0 + \omega_1 - i\eta} \right. \\ \left. - \frac{\langle n | \hat{c}_{\mathbf{k}_1\sigma_1} | m \rangle \langle m | \hat{c}_{\mathbf{k}_2\sigma_2} | 0 \rangle}{E_m - E_0 + \omega_2 - i\eta} \right\}, \quad (21)$$

with  $E_m$  the  $N - 1$  particle sector eigenvalues.

Note that this expression bears a strong resemblance to the Kramers-Heisenberg expression for resonant inelastic x-ray scattering (RIXS) in which the manifold of  $N - 1$  states  $\{|m\rangle\}$  plays the role of intermediate  $N + 1$  core hole states whereby a core electron is photoexcited into the valence band [8]. While for RIXS the final states have the same number of electrons  $N$  as the initial state as the core hole is refilled via photodeexcitation, the pair photoemission final states have two less electrons  $N - 2$ . Despite their apparent differences, the functional form of Eq. (21) indicates that we would expect resonant pair photoemission whenever one or both of the frequencies  $\omega_{1,2}$  correspond to the  $N - 1$  removal state energies observed in photoemission rather than the core-valence transition energies as in RIXS.

To illustrate the differences between pair photoemission and uncorrelated single-particle photoemission and how information can be obtained from both, we start by reminding readers that the pairing energy  $\Delta(\mathbf{k}_1, \mathbf{k}_2)$  for two momentum states  $\mathbf{k}_{1,2}$  is  $\Delta(\mathbf{k}_1, \mathbf{k}_2) = E_2(\mathbf{k}_1, \mathbf{k}_2) - E_1(\mathbf{k}_1) - E_1(\mathbf{k}_2) + E_0$ , where  $E_{0,1,2}$  denotes the energies of the  $N = 0, 1, 2$  particle removal states, respectively, viz., where single-particle photoemission yielding  $E_1 - E_0$  and pair photoemission  $E_2 - E_0$ . By inspection of Eqs. (20) and (21), we can see that  $E_2 - E_0$  is determined by the overall energy conservation by  $\omega_1 + \omega_2$ . In other words, this is given by the slope of the line connecting  $\omega_1$  and  $\omega_2$  for pair photoemission when plotted as a function of both frequencies. The resonance denominator of Eq. (21) shows that the intensity on this line is modulated when  $\omega_{1,2}$  coincide with the single-particle energies  $E_1 - E_0$  observed in single-particle photoemission.

### D. Retarded pairing correlator

Suppose that the measured pair-emission signal is obtained as a function of sum and difference frequencies:

$$\omega = \omega_1 + \omega_2, \quad \Delta\omega = \omega_1 - \omega_2. \quad (22)$$

By inspection of Eq. (18), one can see that the difference frequency  $\Delta\omega$  parameterizes the retardation of the pair-emission process from the sample, i.e., the time delay between emission of the first and second electron of an observed pair. Integration over the difference frequency  $\Delta\omega$  then yields

$$D_{\mathbf{k}_1, \mathbf{k}_2}^{(0)}(\omega) = \int_{-\infty}^{\infty} d\Delta\omega D_{\mathbf{k}_1, \mathbf{k}_2}^{(0)}\left(\frac{\omega + \Delta\omega}{2}, \frac{\omega - \Delta\omega}{2}\right) \\ = \int_{-\infty}^{\infty} dt e^{-i\omega t} \int_{-\infty}^{\infty} d\tau \langle \hat{c}_{\mathbf{k}_1}^\dagger(t) \hat{c}_{\mathbf{k}_2}^\dagger(t + \tau) \hat{c}_{\mathbf{k}_1}(\tau) \hat{c}_{\mathbf{k}_1}(0) \rangle, \quad (23)$$

which can be straightforwardly expressed as a spectral decomposition

$$D_{\mathbf{k}_1\mathbf{k}_2}^{(0)}(\omega) = \sum_{n,m} \delta(\omega + E_0 - E_n) |\langle n | \hat{c}_{\mathbf{k}_1} | m \rangle \langle m | \hat{c}_{\mathbf{k}_2} | 0 \rangle|^2. \quad (24)$$

Thus, coincidence pair ARPES can yield the dynamic superconducting pairing susceptibility. In a BCS superconductor, the resulting response has a peak at finite  $\omega$  that corresponds to the momentum-dependent superconducting gap. Spin-resolved pairing as well as pairing that can occur at finite momenta corresponding to a pair density wave was recently examined in Ref. [9]. Importantly, coincidence pair ARPES can also provide measurements for the dynamic pair susceptibility in materials at temperatures above the ordered phase or for systems that may be highly frustrated or condense into a different nonsuperconducting pair state. While dynamic pairing correlations have been measured via different numerical methods, such as determinant quantum Monte Carlo, for example [10,11], susceptibility measurements have been lacking.

### III. APPLICATIONS

#### A. Free electrons

If the valence electrons within the sample are free, the four-point function factorizes to

$$G_{\mathbf{k}_1\mathbf{k}_2}^{(2)}(\tau_1, \tau'_1, \tau'_2, \tau_2) \rightarrow G_{\mathbf{k}_1}^<(\tau_1 - \tau_2) G_{\mathbf{k}_2}^<(\tau'_1 - \tau'_2), \quad (25)$$

for  $\mathbf{k}_1 \neq \mathbf{k}_2$  and suppressed spin indices. The coincidence detection rate becomes a product of single-particle ARPES detection rates:

$$D_{\mathbf{k}_1\mathbf{k}_2}^{(0)}(\omega_1, \omega_2) \rightarrow P_{\mathbf{k}_1}(\omega_1) P_{\mathbf{k}_2}(\omega_2), \quad (26)$$

which only contributes if the quantum numbers of the photodetected electrons are not identical due to Pauli exclusion. This is a useful check to determine the overall magnitude of the pair ARPES compared with single-particle ARPES and can help to assess the spectral intensities of two-particle collective modes separately from the single-particle continuum.

#### B. BCS theory

If the system of interest is well described by a BCS mean field ansatz, the valence band is again composed of free Bogoliubov fermions. In this case, the four-point function factorizes, and the coincidence pair photoemission signal additionally includes a pairing term:

$$D_{\mathbf{k}_1\mathbf{k}_2}^{(0)}(\omega_1, \omega_2) = P_{\mathbf{k}_1}(\omega_1) P_{\mathbf{k}_2}(\omega_2) + |P_{\mathbf{k}_1\mathbf{k}_2}^{\text{pair}}(\omega_1, \omega_2)|^2, \quad (27)$$

where

$$P_{\mathbf{k}_1\mathbf{k}_2}^{\text{pair}}(\omega_1, \omega_2) = \int d\tau d\tau' s(\tau) s(\tau') \exp[i(\omega_1\tau + \omega_2\tau')] \times \langle \mathcal{T} \hat{c}_{\mathbf{k}_1}^\dagger(\tau) \hat{c}_{\mathbf{k}_2}^\dagger(\tau') \rangle \quad (28)$$

is a weighted time average of the time-ordered anomalous Green's function. For the case where the shape functions

$s(t) = 1$ , the BCS singlet pair wave function gives the value:

$$P_{\mathbf{k}_1\mathbf{k}_2}^{\text{pair}}(\omega_1, \omega_2) = \delta(\mathbf{k}_1 + \mathbf{k}_2) \delta(\sigma_1 + \sigma_2) \delta(\omega_1 + \omega_2) \times \frac{\Delta_{\mathbf{k}_1}}{(\omega_1 - i\eta)^2 - E_{\mathbf{k}_1}^2}, \quad (29)$$

with the Bogoliubov energy given by  $E_{\mathbf{k}}^2 = \epsilon_{\mathbf{k}}^2 + \Delta_{\mathbf{k}}^2$  for free particle dispersion  $\epsilon_{\mathbf{k}}$ , and  $\eta$  is a small real quantity [6].

We note that Eq. (29) yields a sharp peak at the Fermi level ( $\omega_1 = \omega_2 = 0$ ) when the delta functions are satisfied, indicating that pair ARPES can be used to detect the underlying Cooper pair structure in terms of center of mass spin (i.e., singlet vs triplet) and momentum (i.e., Fulde-Ferrell-Larkin-Ovchinnikov or pair density-wave states), as has been noted previously [6,9]. Moreover, the fermion momentum dependence of the energy gap  $\Delta(\mathbf{k})$  can be scanned and directly measured.

#### C. Hubbard models for correlated electrons

The single-band Hubbard model may provide a simple way to characterize the behavior of pair photoemission for correlated electrons in systems without superconducting long-range order. Specifically, we will utilize eigenstates of the particle-hole symmetric Hubbard model:

$$H = -t \sum_{(i,j),\sigma} c_{i,\sigma}^\dagger c_{j,\sigma} + U \sum_i \left( n_{i,\uparrow} - \frac{1}{2} \right) \left( n_{i,\downarrow} - \frac{1}{2} \right), \quad (30)$$

on an 8A (diamond) Betts cluster [12] to construct pair ARPES [Fig. 2(a)]. Here,  $c_{i,\sigma}, c_{i,\sigma}^\dagger$  removes, adds a particle at site  $i$  with spin  $\sigma$ ,  $n_{i,\sigma}$  is the particle density per spin at site  $i$ ,  $t$  denotes hybridization between nearest-neighbor sites  $i$  and  $j$ , and  $U$  is a measure of the local interaction between opposite spins. Throughout, we assume units where  $\hbar = 1$ .

While much work has been performed via density matrix renormalization group techniques, for example, to ascertain whether the Hubbard model in the thermodynamic limit harbors superconductivity, our goal is more modest. By examining the eigenstates and constructing pair ARPES on finite clusters, which cannot have a bona fide phase transition, we may be able to highlight how coincidence spectroscopy can be used to quantitatively measure pair field susceptibilities in systems where U(1) gauge symmetry is not broken but fluctuating order may be inferred.

Pairing has been long investigated in exact diagonalization studies of the Hubbard model on small clusters [13–15]. The pair-binding energy  $\Delta$  is defined as the energy difference between the ground-state energies of  $N$  and  $N - 2$  particle systems minus twice the energy of the  $N - 1$  system:

$$\Delta = E_N + E_{N-2} - 2E_{N-1}. \quad (31)$$

A negative  $\Delta$  indicates an effective electron pair attraction.

The pair-binding energy  $\Delta$  obtained for the repulsive and attractive Hubbard model at half-filling  $N_{\text{electrons}} = 8 = N$  is shown in Fig. 2(d). For repulsive  $U$ ,  $\Delta$  is negative for  $U/t \lesssim 8$  and becomes positive for larger values. The ground state of the attractive Hubbard model ( $U < 0$ ) can be well modeled

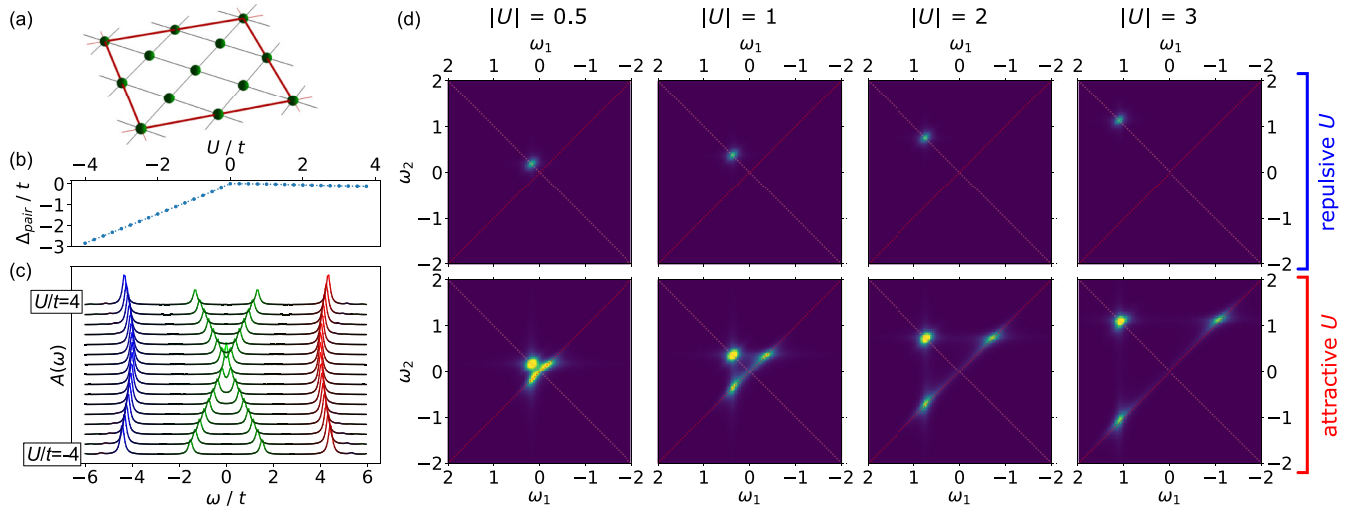


FIG. 2. Pair ARPES for the attractive and repulsive Hubbard model. (a) Schematics of the 8-site Betts cluster. (b) Pair-binding energy as a function of repulsive and attractive Hubbard interactions at half-filling. (c) Single-particle spectrum  $A(\omega)$  as a function of interactions and momentum [blue, green, and red correspond to  $\mathbf{k} = 0, (\pi/2, \pi/2)$ , and  $(\pi, \pi)$ , respectively]. (d) Top and bottom row panels show opposite-spin  $D_{\mathbf{k},-\mathbf{k}}(\omega_1, \omega_2)$  for repulsive and attractive interactions, respectively, from  $|U| = 0.5$  (left) to  $|U| = 3$  (right). Dashed lines (center and difference frequencies) are guides to the eye. All energies are quoted in units of  $t = 1$ . While the main photoemission peak with  $\omega_1 = \omega_2$  identically tracks attractive and repulsive Coulomb interactions, for  $U < 0$ , pair ARPES reveals the pair-breaking intermediate state via the frequency difference spectrum  $\omega_1 = \omega_2$  for  $\omega_1 + \omega_2 = 0$  (bottom row).

as a BCS superconducting paired state [15] and possesses a pair-binding energy that increases with  $|U|$ .

The ARPES spectra are identical for repulsive or attractive  $U$  via particle-hole symmetry. Figure 2(b) depicts the spectral functions as a function of  $U/t$ , with peaks corresponding to the three unique momenta on the 8A Betts cluster  $(0, 0)$ ,  $(\pi/2, \pi/2)$  (sixfold degenerate), and  $(\pi, \pi)$ , shown in blue, green, and red, respectively. As noted previously [16], spectral peaks move to deeper binding energies as  $|U|$  is increased, and the development of the lower Hubbard band can be more clearly observed. While a pairing gap is clearly observable for attractive  $U$ , a superconductor cannot be distinguished from a Mott gap in single-electron ARPES. Indeed, the spectra for positive and negative  $U$  are identical by virtue of particle-hole symmetry. This further motivates investigating pair photoemission, which intrinsically discriminates between pair and density excitations.

By inspection of the denominators in Eq. (21), one can expect that, for pair ARPES, the largest intensity will be obtained for a given  $\mathbf{k}_1, \mathbf{k}_2$  when the energies  $\omega_1, \omega_2$  are tuned to the respective energy positions of ARPES removal spectra, giving roughly a similar pattern to that obtained by simply multiplying the two independent ARPES spectral functions for photoemitted electrons with opposite spin.

We focus only on momentum states lying closest to the chemical potential and consider two-particle removal ARPES spectra for opposite spins and momenta  $\mathbf{k}_{1,2}$  drawn from the six degenerate momentum points  $(\pm\pi/2, \pm\pi/2)$ ,  $(\pi, 0)$ , and  $(0, \pi)$ . Obtaining the eigenstates for the sectors containing  $N_{\text{electrons}} = 8, 7, 6$  allows for the construction of Fermi golden rule pair ARPES spectral functions  $D_{\mathbf{k}_1, \mathbf{k}_2}(\omega_1, \omega_2)$  via Eqs. (20) and (21), or equivalently via Eq. (B2) upon inclusion of the probe shape functions. We focus on spin-resolved pair photoemission spectra; the spin-agnostic response follows via summing equal- and opposite-spin contributions.

The resulting pair photoemission spectra are shown in Fig. 2(d) for  $\mathbf{k}_1 = -\mathbf{k}_2 = (\pi/2, \pi/2)$  and opposite spins  $\sigma_1 = \uparrow, \sigma_2 = \downarrow$ , for both repulsive and attractive interactions. While both cases show a primary peak at equal pair photoemission energies  $\omega_1 = \omega_2$ , corresponding to the particle-hole-symmetric Hubbard gap, a key new feature is the emergence of a pair of additional peaks for the attractive Hubbard model, with  $\omega_1 + \omega_2 = 0$ . These directly probe the pair-breaking intermediate state and can be understood as a two-step process: (1) First, a photon breaks a Cooper pair to photoemit an electron, while leaving an unpaired electron with pair-breaking energy  $2\Delta$  in the sample. (2) Subsequently, the second photon photoemits this unpaired electron while removing the extra intermediate state energy from the sample. As the final state with two electrons removed from a fully paired superconductor has the same energy as the initial state, the total energy  $\omega_1 + \omega_2$  left in the sample by the photoemission process must equal zero; the intermediate pair-breaking state remains encoded in the energy difference  $\omega_1 - \omega_2$ . These observations can be confirmed by comparing the pair photoemission response to uncorrelated pairs of single photoemission processes, depicted in Fig. 3.

The momentum dependence on each of the fermion momenta as well as the net total momentum  $\mathbf{q} = \mathbf{k}_1 + \mathbf{k}_2$  and net spin  $\sigma = \sigma_1 + \sigma_2$  can reveal further information of the pair wave function. Figure 4 plots pair ARPES for different combinations of photoemitted wave vectors and spins, for  $U/t = 3$ , as a function of center  $\omega_1 + \omega_2$  and relative  $\omega_1 - \omega_2$  frequencies. As expected for singlet pairing in the attractive Hubbard model, one immediately finds that equal-spin photoemitted electrons [Fig. 4(b)] lack the pair-breaking peaks at zero center frequency of the opposite-spin response in Fig. 2(d). In contrast, observations of equal-spin pair-breaking peaks in the correlated pair ARPES response would be suggestive of triplet-pairing instabilities. A similar

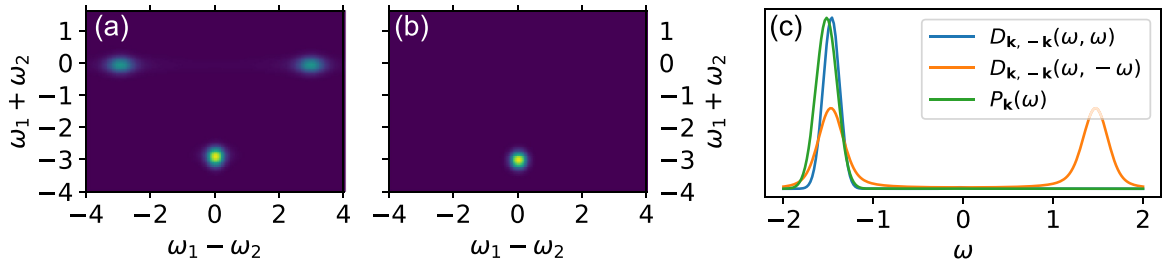


FIG. 3. Comparing single and pair photoemission. (a) and (b) Pair ARPES  $D_{\mathbf{k},-\mathbf{k}}(\omega_1, \omega_2)$  and uncorrelated pairs of single photoemission events  $P_{\mathbf{k}}(\omega_1) \times P_{-\mathbf{k}}(\omega_2)$ , respectively, with line cuts for center and difference frequencies shown in (c). Depicted responses are computed for attractive interactions  $U/t = -3$  with shape function broadening  $\sigma = 4/t$ .

argument follows for photoemitted pairs of electrons with equal momentum  $\mathbf{k}_1 = \mathbf{k}_2$ , as shown in Figs. 4(c) and 4(d); here, an observation of zero-frequency side peaks would be indicative of finite-momentum pairing [17]. Pair photoemission for other momenta remains strongly suppressed [Figs. 4(e)–4(h)] for attractive interactions.

It is expected that these results will be affected by the finite size and geometry of the small cluster as well as adding symmetry-breaking terms, such as  $t'$ , that can break momentum degeneracies. For example, the pair-field correlator obtained for the same Hamiltonian on a  $4 \times 2$  cluster that breaks  $C4$  symmetry, increasing the number of nondegenerate momentum points from 3 in the  $8A$  cluster to 6, has quantitatively the same results for attractive and repulsive  $|U| = 4t$ . The largest low-frequency contribution is for pair momenta  $\mathbf{q} = (\pi, 0)$  and  $(\pi/2, \pi)$ . By including a negative next-nearest hopping  $t' = -0.25t$ , the low-energy pair field correlations are largest for  $\mathbf{q} = (\pi, 0)$  and  $(0, \pi)$  for  $U = 4t$ , while for

$U = -4t$ ,  $\mathbf{q} = (0, 0)$  is still largest. These effects for larger clusters and different geometries should be further addressed.

Lastly, here, we have restricted consideration to zero temperature pair ARPES. One key application of pair ARPES could be to approach ordered phases from high temperature to measure how pair field correlations develop, either toward a true superconducting transition or averted by the onset of another competing order, such as charge and/or spin-density waves [18]. As these phases all appear to have nearly the same ground-state energies in simulations of the Hubbard model, an experimental investigation may provide finer insight into which terms may be missing from the Hubbard model that could formulate closer contact to materials such as the high-temperature superconductors.

In summary, we have presented a theory for pair ARPES whereby two photons produce two photoelectrons detected in coincidence, resolved in both energy and momentum. The corresponding two-particle removal spectra can thus be exploited

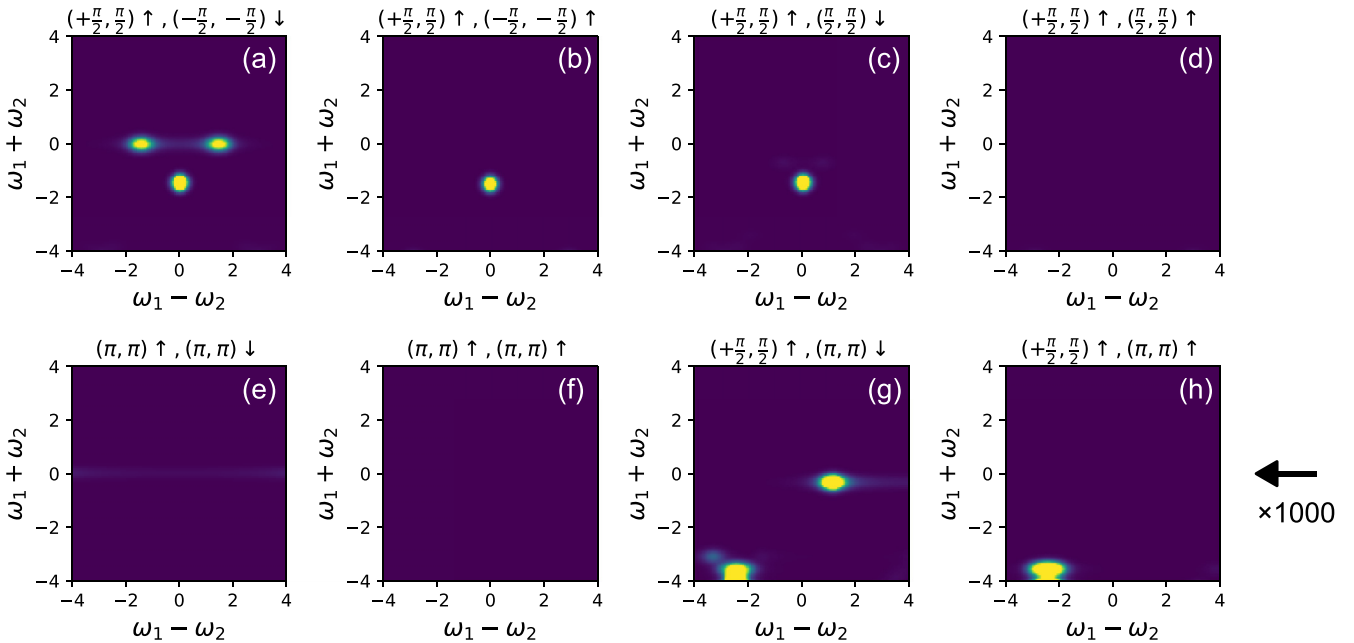


FIG. 4. Spin and momentum dependence of pair ARPES. (a)–(d) Top rows depict the pair ARPES response for the attractive Hubbard model  $U/t = -3$ , for equal/opposite spin and momentum combinations of the momenta  $(\pm\pi/2, \pm\pi/2)$  used in Fig. 2. (e)–(h) Bottom rows depict the subdominant pair ARPES response for other momenta (scaled by a factor of 1000 with respect to the top row), for equal and opposite emitted spins.

to determine the effects of electron correlations in a direct way. The calculated pair response for the attractive and repulsive Hubbard model at half-filling for an 8-site Betts cluster shows spectroscopically how prominent ordering tendencies of superconductivity and the net pair momentum and spin can be inferred directly from experiments.

Experimentally, to make data as close to superconducting pair correlation function as possible, one should try to eject the electron pair from the sample at the same time. In such an instantaneous event, two photons eject two electrons in an interacting volume, for example, a Cooper pair in a superconductor or a pair in a Mott insulator that are sufficiently entangled. In a Cooper pair, this means two electrons within the superconducting coherence volume. In a Mott insulator, assuming that the Hubbard model is a reasonable starting point, this means two electrons not far from each other so that a cascade of local interactions can entangle the electrons. Our theoretical calculation was carried out in a small cluster such that the entanglement is naturally strong.

Such pair photoemission is an experiment with many technical challenges. However, several recent technological advances make it realistic. The first is the emergence of much improved and suitable light sources, such as UV lasers,

high harmonic generation, free electron lasers, and photon focusing schemes. Photons within a very short pulse, such as tens of femtoseconds, can be considered as identical and instantaneous within TOF spectrometers having picosecond resolution. The second is a TOF-based three-dimensional ARPES platform, such as the momentum microscope and its spin-filtered variant. The third is the development of two-dimensional ultrafast multichannel detectors. With time and through an integration of these important technologies, enhanced by timing, energy, momentum discrimination schemes, and machine learning algorithms to improve the signal-to-noise ratio, this spectroscopy may be developed in the near future.

## ACKNOWLEDGMENTS

The authors would like to thank Frank Marsiglio and Joseph Orenstein for insightful discussions. MZ, JEM, DM, FM, PA, ZXS, and TPD acknowledge support from the U.S. Department of Energy, Office of Basic Energy Sciences, Division of Materials Sciences and Engineering, and through Contract No. DE-AC02-05-CH11231 via the Quantum Materials program (KC2202) (JEM).

## APPENDIX A: TWO-PHOTON PAIR PHOTOEMISSION

The main text presents a formal expression of the pair photoemission response [Eq. (13)] which assumes negligible back action between photoemitted electrons and sample electrons. Starting from the second-order perturbative expression:

$$\begin{aligned}
D_{\mathbf{k}_1\mathbf{k}_2} = & \int_{-\infty}^t d\tau_1 d\tau_2 \int_{-\infty}^{\tau_1} d\tau'_1 \int_{-\infty}^{\tau_2} d\tau'_2 s(\tau_1)s(\tau'_1)s(\tau_2)s(\tau'_2) \int d\mathbf{r}_1 d\mathbf{r}'_1 d\mathbf{r}_2 d\mathbf{r}'_2 \int d\mathbf{x}_1 d\mathbf{x}'_1 d\mathbf{x}_2 d\mathbf{x}'_2 \\
& \times \phi_{\mathbf{k}_1}^*(\mathbf{x}_1)\phi_{\mathbf{k}_2}^*(\mathbf{x}'_1)\phi_{\mathbf{k}_2}(\mathbf{x}'_2)\phi_{\mathbf{k}_1}(\mathbf{x}_2) \exp[i\omega_{\text{ph}}(\tau_1 + \tau'_1 - \tau_2 - \tau'_2)] g^*(\mathbf{r}_1)g^*(\mathbf{r}'_1)g(\mathbf{r}'_2)g(\mathbf{r}_2) \\
& \times \sum_{\sigma_1\sigma'_1\nu} \sum_{\sigma_2\sigma'_2\nu'} \langle \hat{\Phi}_{\sigma_1}^\dagger(\mathbf{r}_1, \tau_1)\hat{\Psi}_{\sigma_1}(\mathbf{r}_1, \tau_1)\hat{\Phi}_{\sigma'_1}^\dagger(\mathbf{r}'_1, \tau'_1)\hat{\Psi}_{\sigma'_1}(\mathbf{r}'_1, \tau'_1)\hat{\Psi}_{\nu}^\dagger(\mathbf{x}_1, t)\hat{\Psi}_{\nu'}^\dagger(\mathbf{x}'_1, t) \\
& \times \hat{\Psi}_{\nu'}(\mathbf{x}'_2, t)\hat{\Psi}_{\nu}(\mathbf{x}_2, t)\hat{\Psi}_{\sigma'_2}^\dagger(\mathbf{r}'_2, \tau'_2)\hat{\Phi}_{\sigma'_2}(\mathbf{r}'_2, \tau'_2)\hat{\Psi}_{\sigma_2}^\dagger(\mathbf{r}_2, \tau_2)\hat{\Phi}_{\sigma_2}(\mathbf{r}_2, \tau_2) \rangle, \tag{A1}
\end{aligned}$$

neglecting back action on the sample permits a decomposition:

$$\begin{aligned}
D_{\mathbf{k}_1\mathbf{k}_2} = & \sum_{\sigma_1\sigma'_1\nu} \sum_{\sigma_2\sigma'_2\nu'} \int_{-\infty}^t d\tau_1 d\tau_2 \int_{-\infty}^{\tau_1} d\tau'_1 \int_{-\infty}^{\tau_2} d\tau'_2 s(\tau_1)s(\tau'_1)s(\tau_2)s(\tau'_2) \exp[i\omega_{\text{ph}}(\tau_1 + \tau'_1 - \tau_2 - \tau'_2)] \\
& \times \int d\mathbf{r}_1 d\mathbf{r}'_1 d\mathbf{r}_2 d\mathbf{r}'_2 g^*(\mathbf{r}_1)g^*(\mathbf{r}'_1)g(\mathbf{r}'_2)g(\mathbf{r}_2) \langle \hat{\Phi}_{\sigma_1}^\dagger(\mathbf{r}_1, \tau_1)\hat{\Phi}_{\sigma'_1}^\dagger(\mathbf{r}'_1, \tau'_1)\hat{\Phi}_{\sigma'_2}(\mathbf{r}'_2, \tau'_2)\hat{\Phi}_{\sigma_2}(\mathbf{r}_2, \tau_2) \rangle \\
& \times \int d\mathbf{x}_1 d\mathbf{x}'_1 \phi_{\mathbf{k}_1}^*(\mathbf{x}_1)\phi_{\mathbf{k}_2}^*(\mathbf{x}'_1) \langle \hat{\Psi}_{\sigma_1}(\mathbf{r}_1, \tau_1)\hat{\Psi}_{\sigma'_1}(\mathbf{r}'_1, \tau'_1)\hat{\Psi}_{\nu}^\dagger(\mathbf{x}_1, t)\hat{\Psi}_{\nu'}^\dagger(\mathbf{x}'_1, t) \rangle \\
& \times \int d\mathbf{x}_2 d\mathbf{x}'_2 \phi_{\mathbf{k}_2}(\mathbf{x}'_2)\phi_{\mathbf{k}_1}(\mathbf{x}_2) \langle \hat{\Psi}_{\nu'}(\mathbf{x}'_2, t)\hat{\Psi}_{\nu}(\mathbf{x}_2, t)\hat{\Psi}_{\sigma'_2}^\dagger(\mathbf{r}'_2, \tau'_2)\hat{\Psi}_{\sigma_2}^\dagger(\mathbf{r}_2, \tau_2) \rangle. \tag{A2}
\end{aligned}$$

Suppose now that the sample electrons near the Fermi energy are confined to a single valence band  $\hat{\Phi}_\sigma(\mathbf{r}, \tau) \approx \frac{1}{\sqrt{L}} \sum_{\mathbf{k}} u_{\mathbf{k}}(\mathbf{r})\hat{c}_{\mathbf{k}\sigma}(\tau)e^{i\mathbf{k}\mathbf{r}}$  with Bloch function  $u_{\mathbf{k}}(\mathbf{r})$ . Expanding the photoemitted electron fields in a plane-wave basis and Fourier-transforming the detector form factors  $\phi_{\mathbf{k}}(\mathbf{x}) = \int d\mathbf{p}e^{-i\mathbf{p}\mathbf{x}}\phi_{\mathbf{k}}(\mathbf{p})$ , one obtains

$$\begin{aligned}
D_{\mathbf{k}_1\mathbf{k}_2} = & \sum_{\sigma_1\sigma'_1\nu} \sum_{\sigma_2\sigma'_2\nu'} \int_{-\infty}^t d\tau_1 d\tau_2 \int_{-\infty}^{\tau_1} d\tau'_1 \int_{-\infty}^{\tau_2} d\tau'_2 s(\tau_1)s(\tau'_1)s(\tau_2)s(\tau'_2) \exp[i\omega_{\text{ph}}(\tau_1 + \tau'_1 - \tau_2 - \tau'_2)] \\
& \times \int d\mathbf{k} d\mathbf{k}' d\mathbf{q} \langle \hat{c}_{\mathbf{k},\sigma_1}^\dagger(\tau_1)\hat{c}_{\mathbf{q}-\mathbf{k},\sigma'_1}^\dagger(\tau'_1)\hat{c}_{\mathbf{q}-\mathbf{k}',\sigma'_2}(\tau'_2)\hat{c}_{\mathbf{k}',\sigma_2}(\tau_2) \rangle
\end{aligned}$$



$$\begin{aligned}
& \times \int_{\text{BZ}} d\mathbf{r}_1 d\mathbf{r}'_1 d\mathbf{r}_2 d\mathbf{r}'_2 g^*(\mathbf{r}_1) g^*(\mathbf{r}'_1) g(\mathbf{r}'_2) g(\mathbf{r}_2) u_{\mathbf{k}}^*(\mathbf{r}_1) u_{\mathbf{q}-\mathbf{k}}^*(\mathbf{r}'_1) u_{\mathbf{q}-\mathbf{k}}(\mathbf{r}'_2) u_{\mathbf{k}}(\mathbf{r}_2) \\
& \times \int d\mathbf{p} \phi_{\mathbf{k}_1}^*(\mathbf{q}-\mathbf{p}) \phi_{\mathbf{k}_2}^*(\mathbf{p}) \langle \hat{\Psi}_{\sigma_1}(\mathbf{k}, \tau_1) \hat{\Psi}_{\sigma'_1}(\mathbf{q}-\mathbf{k}, \tau'_1) \hat{\Psi}_{\nu'}^\dagger(\mathbf{q}-\mathbf{p}, t) \hat{\Psi}_{\nu'}^\dagger(\mathbf{p}, t) \rangle \\
& \times \int d\mathbf{p}' \phi_{\mathbf{k}_2}(\mathbf{p}') \phi_{\mathbf{k}_1}(\mathbf{q}-\mathbf{p}') \langle \hat{\Psi}_{\nu'}(\mathbf{p}', t) \hat{\Psi}_{\nu}(\mathbf{q}-\mathbf{p}', t) \hat{\Psi}_{\sigma'_2}^\dagger(\mathbf{q}-\mathbf{k}', \tau'_2) \hat{\Psi}_{\sigma_2}^\dagger(\mathbf{k}', \tau_2) \rangle.
\end{aligned} \tag{A3}$$

Rewriting the third line in terms of matrix elements recovers the expression presented in the main text.

## APPENDIX B: SPECTRAL REPRESENTATION OF PAIR ARPES

A useful representation of pair ARPES that accounts for the probe shape function follows from a spectral decomposition of Eq. (18):

$$\begin{aligned}
D_{k_1, k_2}^{(0)}(\omega_1, \omega_2) &= \sum_n \left| \int_{-\infty}^{\infty} dt \int_0^{\infty} dt' s(t) s(t-t') \sum_m [\langle n | \hat{c}_{\mathbf{k}_1} | m \rangle \langle m | \hat{c}_{\mathbf{k}_2} | 0 \rangle \exp(i\omega_1 t') - \langle n | \hat{c}_{\mathbf{k}_2} | m \rangle \langle m | \hat{c}_{\mathbf{k}_1} | 0 \rangle \exp(i\omega_2 t')] \right. \\
& \times \left. \exp\{i[(\epsilon_n - \epsilon_0 - \omega_1 - \omega_2)t - (\epsilon_n - \epsilon_m)t']\} \right|^2,
\end{aligned} \tag{B1}$$

with  $s(t)$  the Gaussian shape functions. The time integrals can now be evaluated, and one arrives at

$$D_{k_1, k_2}^{(0)}(\omega_1, \omega_2) = \sum_n \left| \sum_m [\langle n | \hat{c}_{\mathbf{k}_1} | m \rangle \langle m | \hat{c}_{\mathbf{k}_2} | 0 \rangle X_{nm}(\omega_1, \omega_2) - \langle n | \hat{c}_{\mathbf{k}_2} | m \rangle \langle m | \hat{c}_{\mathbf{k}_1} | 0 \rangle X_{nm}(\omega_2, \omega_1)] \right|^2, \tag{B2}$$

where

$$\begin{aligned}
X_{nm}(\omega_1, \omega_2) &= \sigma^2 \exp\left[-\frac{\sigma^2}{4}(\omega_1 + \omega_2 + \epsilon_0 - \epsilon_n)^2\right] \left\{ \frac{1}{2} \exp\left[-\frac{\sigma^2}{4}(\omega_2 - \omega_1 + \epsilon_0 + \epsilon_n - 2\epsilon_m)^2\right] \right. \\
& \left. + \frac{i}{\sqrt{\pi}} \mathcal{D}_+\left[\frac{\sigma}{2}(\omega_2 - \omega_1 + \epsilon_0 + \epsilon_n - 2\epsilon_m)\right] \right\}.
\end{aligned} \tag{B3}$$

Here,  $\sigma$  is the Gaussian broadening of the shape function, and  $\mathcal{D}_+(x)$  denotes the Dawson function, which is related to the error function  $\mathcal{D}_+(x) = \sqrt{\pi/4} \exp(-x^2) \text{erfi}(x)$ .

- 
- [1] J. A. Sobota, Y. He, and Z.-X. Shen, *Rev. Mod. Phys.* **93**, 025006 (2021).  
[2] J. Berakdar, *Phys. Rev. B* **58**, 9808 (1998).  
[3] G. A. Sawatzky, *Treatise Mater. Sci. Technol.* **30**, 167 (1988).  
[4] G. A. van Riessen, Z. Wei, R. S. Dhaka, C. Winkler, F. O. Schumann, and J. Kirschner, *J. Phys.: Condens. Matter* **22**, 092201 (2010).  
[5] N. Fominykh, J. Berakdar, and J. Henk, and P. Bruno, *Phys. Rev. Lett.* **89**, 086402 (2002).  
[6] Y. Su, and C. Zhang, *Phys. Rev. B* **101**, 205110 (2020).  
[7] J. K. Freericks, H. R. Krishnamurthy, and T. Pruschke, *Phys. Rev. Lett.* **102**, 136401 (2009).  
[8] L. J. P. Ament, M. van Veenendaal, T. P. Devereaux, J. P. Hill, and J. van den Brink, *Rev. Mod. Phys.* **83**, 705 (2011).  
[9] F. Mahmood, T. Devereaux, Peter Abbamonte, and D. K. Morr, *Phys. Rev. B* **105**, 064515 (2022).  
[10] T. A. Maier and D. J. Scalapino, *npj Quantum Mater.* **4**, 30 (2019).  
[11] E. W. Huang, W. O. Wang, J. K. Ding, T. Liu, F. Liu, X.-X. Huang, B. Moritz, and T. P. Devereaux, *J. Phys. Soc. Jpn.* **90**, 111010 (2021).  
[12] D. Betts, H. Lin, and J. Flynn, *Can. J. Phys.* **77**, 353 (1999).  
[13] H. Q. Lin, J. E. Hirsch, and D. J. Scalapino, *Phys. Rev. B* **37**, 7359 (1988).  
[14] J. A. Riera and A. P. Young, *Phys. Rev. B* **39**, 9697 (1989).  
[15] F. Marsiglio, *Phys. Rev. B* **55**, 575 (1997).  
[16] E. Dagotto, R. Joynt, A. Moreo, S. Bacci, and E. Gagliano, *Phys. Rev. B* **41**, 9049 (1990); E. Dagotto, A. Moreo, F. Ortolani, J. Riera, and D. J. Scalapino, *Phys. Rev. Lett.* **67**, 1918 (1991); E. Dagotto, F. Ortolani, and D. J. Scalapino, *Phys. Rev. B* **46**, 3183 (1992).  
[17] See, e.g., D. F. Agterberg, J. C. S. Davis, S. D. Edkins, E. Fradkin, D. J. Van Harlingen, S. A. Kivelson, P. A. Lee, L. Radzihovsky, J. M. Tranquada, and Y. Wang, *Annu. Rev. Condens. Matter Phys.* **11**, 231 (2020).  
[18] J. T. Anderson and A. M. Goldman, *Phys. Rev. Lett.* **25**, 743 (1970); N. Bergeal, J. Lesueur, M. Aprili, G. Faini, J. P. Contour, and B. Leridon, *Nat. Phys.* **4**, 608 (2008).